Article

Quantification of Lipid Corona Formation on Colloidal Nanoparticles from Lipid Vesicles

Xi Zhang, Arun Kumar Pandiakumar, Robert J Hamers, and Catherine J. Murphy

Anal. Chem., **Just Accepted Manuscript** • DOI: 10.1021/acs.analchem.8b03911 • Publication Date (Web): 14 Nov 2018

Quantification of Lipid Corona Formation on Colloidal Nanoparticles from Lipid Vesicles

Xi Zhang†, Arun Kumar Pandiakumar‡, Robert J. Hamers‡ and Catherine J. Murphy*†

† Department of Chemistry, University of Illinois at Urbana-Champaign, 600 S. Mathews Ave., Urbana, Illinois 61801, United States

‡ Department of Chemistry, University of Wisconsin—Madison, 1101 University Avenue, Madison, Wisconsin 53706, United States

*to whom correspondence should be addressed: murphycj@illinois.edu

ABSTRACT

Formation of a protein corona around nanoparticles when immersed into biological fluids is well-known; less studied is the formation of lipid coronas around nanoparticles. In many cases, the identity of a nanoparticle-acquired corona determines nanoparticle fate within a biological system and its interactions with cells and organisms. This work systematically explores the impact of nanoparticle surface chemistry and lipid character on the formation of lipid coronas for three different nanoparticle surface chemistries (two cationic, one anionic) on 14 nm gold nanoparticles exposed to a series of lipid vesicles of four different compositions. Qualitative (plasmon band shifting, ζ potential analysis, dynamic light scattering on the part of the nanoparticles) and quantitative (lipid liquid chromatography/mass spectrometry) methods are developed with a "pull-down" scheme to assess the degree of lipid corona formation in these systems. In general, cationic nanoparticles extract 60-95% of the lipids available in vesicles under the described experimental conditions, while anionic nanoparticles extract almost none. While electrostatics apparently dominate the lipid-nanoparticle interactions, primary amine polymer surfaces extract more lipids

than quaternary ammonium surfaces. Free cationic species can act as lipid-binding competitors in solution.

INTRODUCTION

Nanotechnology is one of the enabling technologies of the twenty-first century. Much progress has been made in controlling material composition and structure at the nanoscale, which leads to control of the physicochemical properties and function of nanomaterials.[1] In particular, gold nanoparticles (AuNPs) are of particular interest due to their relative chemical inertness, versatile surface chemistry, and unique optical properties, allowing applications in diagnostics, imaging, drug delivery, and therapeutics.[2–7] In the context of these biological applications, knowledge of the interaction of nanomaterials with biomolecules, cells, and organisms is critical,[8,9] and concerns about potential environmental, health, and safety issues have been raised.[10–12] How do nanomaterials interact with their surroundings, and what are the molecular mechanisms driving those interactions? Answers to these questions will improve the design of nanomaterials to retain function while minimizing detrimental effects.[13,14]

When nanoparticles are exposed to biological or natural environments, they are known to acquire a coating ("corona") of biomolecules.[15–17] While much work to date has focused on protein coronas, fewer studies examine other biomolecular coronas such as lipid coronas.[18,19] In one recent example, lipids, along with proteins, were found to attach to nanoparticles when interacting with pulmonary surfactant.[19] Also, computational simulations suggest that lipid coronas form on nanoparticles with specific surface chemistries.[20–22]

Since cellular membranes are composed primarily of phospholipid bilayers, forming the frontier

between the cell and its environment,[23] the membrane can be considered as one of the initial points of contact between a nanomaterial and a living system. Supported lipid bilayers and suspended lipid vesicles are commonly used as models for phospholipid cell membranes; suspended lipid vesicles are good models for intracellular organelles.[24–28] Recent collaborative work from our laboratory showed lipid corona formation on polycation-wrapped gold nanoparticles upon interaction with anionic supported lipid bilayers via several techniques including ζ-potential measurement, single molecule imaging, and molecular dynamics simulations.[29] Analysis of colloidal nanoparticles via centrifugation-based assays have been used to determine corona-nanoparticle interactions.[30,31]

Developing quantitative relationships between observables can help predict the biological responses to nanoparticles and eventually assist in uncovering the fundamental mechanisms of nano-bio interactions.[32] Therefore, the goal of this study is to quantify the degree of lipid binding to nanoparticles in colloidal solution: the lipids are in the form of vesicles, to simulate organelles. A centrifugation-based pull-down assay was developed wherein three AuNPs were incubated with suspended phospholipid vesicles of varied composition; lipids associated with the AuNPs were pulled down via centrifugation, and remaining lipids were left in the supernatant. UV-visible spectroscopy, dynamic light scattering (DLS), and laser Doppler electrophoresis measurements were performed on the AuNPs, while quantitative liquid chromatography-tandem mass spectrometry (LC-MS/MS) experiments quantified lipids in each fraction.

MATERIALS AND METHODS

Materials. Gold(III) chloride trihydrate ($HAuCl_4 \cdot 3H_2O$, ≥99.9%), sodium citrate tribasic dihydrate ($Na_3Ct \cdot 2H_2O$, ≥99%), poyl(allylamine) hydrochloride (PAH) (~17500 g mol^{-1}), sodium chloride

(NaCl), and (4-(2-hydroxyethyl)-1-piperazineethanesulfonic acid) (HEPES) were obtained from Sigma-Aldrich and used as received. 16-(Mercaptohexadecyl)trimethylammonium bromide (MTAB) was prepared according Zubarev *et al.*(see Supporting Information for detailed procedures and characterization).[33] The lipids 1,2-dioleoyl-sn-glycero-3-phosphocholine (DOPC), 1,2-dioleoyl-sn-glycero-3-phospho-L-serine (DOPS), 1,2-dioleoyl-sn-glycero-3-phospho-(1'-rac-glycerol (DOPG), 1,2-dioleoyl-sn-glycero-3-phosphoethanolamine (DOPE) were purchased from Avanti Polar Lipids. All solutions were prepared in 18 MΩ·cm nanopure water. Glassware was cleaned prior to synthesis using aqua regia (*Caution!*) and then rinsed with nanopure water.

Citrate-AuNPs synthesis. We synthesized AuNPs of 14 nm diameter, capped with citrate, by the Turkevich method.[34] Briefly, 1.25 mL of 0.1 M $HAuCl_4 \cdot 3H_2O$ was added to 498.75 mL of ultrapure water, and the solution was heated to a rolling boil. Then, 10 mL of 1% w/w sodium citrate was added, and the solution was kept boiling for an additional 40 min. After the heat was turned off, the solution was allowed to cool naturally, and an additional 2.5 mL of 1% w/w sodium citrate was added. To purify, the AuNPs were centrifuged at 8000*g* for 20 min twice unless stated otherwise. The supernatant was discarded, and the remaining sample was redispersed in nanopure water. To calculate concentrations of the AuNPs, an extinction coefficient of 2.18×10^8 M^{-1} cm^{-1} was used.[35]

Wrapping Citrate-AuNPs with PAH. A 20 mL solution of 2 nM Citrate-AuNPs was prepared in a 50 mL centrifuge tube. In another tube, 2 mL of 0.01 M NaCl was mixed with 4 mL of 10 mg mL^{-1} PAH. The PAH solution was then added to the AuNP solution. The tube was placed on a BellyDancer shaker overnight to mix, and the nanoparticle solution was purified by centrifugation at 8000*g* for 20 min twice unless stated otherwise. The final pellet of PAH-AuNPs was resuspended in 10 mM HEPES buffer (1 mM NaCl, pH 7.4).

Coating Citrate-AuNPs with MTAB. A 1.0 mL aqueous solution of 1.5 mg mL^{-1} MTAB was heated at 60 °C for 30 min to achieve dissolution. Subsequently, 0.30 mL of 300 nM 15 nm AuNPs were added to the MTAB solution. The solution was kept at 60 °C overnight and purified by centrifugation at 8000*g* for 20 min twice unless stated otherwise. The final pellet of MTAB-AuNPs was resuspended in 10 mM HEPES buffer (1 mM NaCl, pH 7.4).

Lipid vesicle preparation. Small unilamellar vesicles were prepared by a sonication method previously described by the Morrissey Lab at UIUC (https://tf7.org/suv.pdf). Briefly, lipid mixtures in chloroform were combined to the desired ratio (pure DOPC, 9:1 DOPC/DOPS, 9:1 DOPC/DOPG, 9:1 DOPC/DOPE), and vortexed for 30 s in a glass vial to achieve a homogenous mixture. The solvent was evaporated under a stream of ultrapure N_2 gas, and the dried film was placed in vacuum for additional 2 h. The dried lipid film was rehydrated to a 1 mg mL^{-1} stock solution in 10 mM HEPES buffer (1 mM NaCl, pH 7.4) for 1 h. The rehydrated lipid solution was vortexed for 1 min to a milky solution, then was placed in a bath sonicator until the suspension changes from milky to nearly clear in appearance (~15 min for DOPC/DOPG and DOPC/DOPS, ~30 min for DOPC and DOPC/DOPE). Final lipid vesicle solutions were stored at 4 °C and used within 2 days. The lipid vesicles were characterized by DLS and laser Doppler electrophoresis.

Nanoparticle and lipid vesicles interactions. All experiments and analyses were conducted in 10 mM HEPES buffer (1 mM NaCl, pH 7.4). In a typical experiment, unless stated otherwise, 500 µL 2.4 nM AuNPs were added to 500 µL 1 µg mL^{-1} diluted as-prepared lipid vesicles in glass vials. Controls were done with an equivalent of same buffer in place of the colloidal gold solution, which take into account any potential losses of lipids due to adsorption to vials, etc. during processing. The combined solutions were mixed gently well before storage at room temperature overnight

(~18h) to achieve equilibrium. All samples were prepared in triplicate. After incubation, the solutions were transferred to 1.5 mL Eppendorf tubes and centrifuged at 16,000*g* for 50 min to achieve a clear separation. The AuNPs were redispersed in buffer and characterized by several methods, while the supernatants, containing free lipids, were quantified via LC-MS/MS. The concentration of lipids bound to AuNPs was equated, by mass balance, to the concentration in the control (C_{total}) minus the concentration in the supernatant ($C_{supernatant}$) to get the concentration of nanoparticle-bound lipids (C_{bound}), and bound lipid percentage of total (C_{bound}/C_{total}).

Nanoparticle and lipid vesicle characterization and instrumentation. Absorption spectra of all AuNPs were taken on a Cary 500 scan UV−vis−near-IR spectrophotometer. Transmission electron microscopy (TEM) data of AuNPs were obtained with a JEOL 2100 cryo electron microscope operating at 200 kV. DLS and laser Doppler electrophoresis were conducted on a Brookhaven ZetaPALS instrument. For lipid quantification, samples were analyzed with a 5500 QTRAP LC/MS/MS system (Sciex, Framingham, MA) in the Metabolomics Lab of the Roy J. Carver Biotechnology Center, University of Illinois at Urbana-Champaign. Details are described in the Supporting Information.

RESULTS AND DISCUSSION

For this study, 14 nm diameter AuNPs with either an anionic ligand: sodium citrate (Citrate-AuNPs) or two different cationic ligands: 16-mercaptohexadecyltrimethylammonium bromide (MTAB-AuNPs) or poyl(allylamine) hydrochloride (PAH-AuNPs) were studied. MTAB displays a quaternary ammonium group to the solvent while PAH displays primary amines (Figure 1). We chose PAH as a coating because it is a common polyelectrolyte wrapping for nanoparticles, widely

used in studies concerning nanoparticle organismal toxicity, lipid membrane interactions, and more.[36–38] In previous studies in our group, we found PAH-AuNPs promoted protein aggregation and beta-sheet formation whereas MTAB-AuNPs did not, even when the AuNPs possessed similar ζ-potentials, suggesting that protein behavior on NPs cannot be predicted by surface potential alone.[39,40] The question, then, is to what extent do lipids also distinguish molecular-level details of nanoparticle surfaces. The suspended lipid vesicles were made in four combinations: pure zwitterionic DOPC, and DOPC containing 10% anionic DOPS, anionic DOPG, or zwitterionic DOPE. These DOPC-rich lipid vesicles were chosen because the zwitterionic PC headgroup is one of the most abundant headgroups in biological membranes.[41,42]

The workflow for the lipid corona-nanoparticle experiments is shown in Figure 1e.

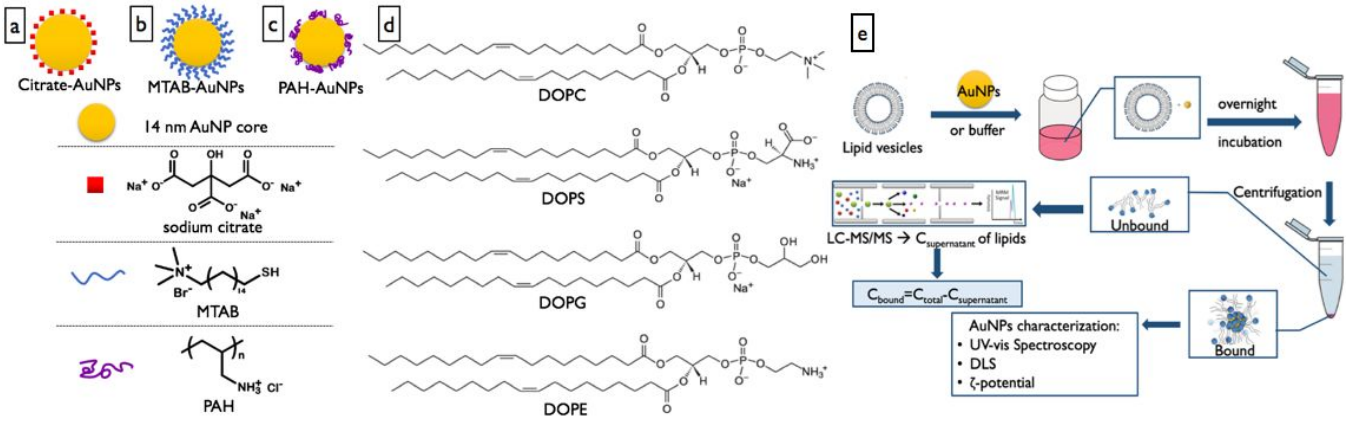

Figure 1. Schematic of a) Citrate-AuNPs, b) MTAB-AuNPs, c) PAH-AuNPs, d) structures of lipids, e) Experimental workflow for quantification of lipid coronas on gold nanoparticles. After incubation with lipid vesicles, gold nanoparticles are centrifuged to separate free from bound lipid. Lipid quantification is performed by LC-MS/MS in the supernatants compared to standards in the same buffer system as the original incubation; total lipid – free lipids = bound lipids. Figures are

not drawn to scale, and the state of the lipids upon and after incubation with nanoparticles (vesicle vs. free) is not known.

AuNPs and lipid vesicle characterizations. All AuNPs before lipid incubation were well characterized. The UV-vis spectra of representative batches of Citrate-AuNPs, MTAB-AuNPs and PAH-AuNPs are shown in Figure S1. The plasmon band maximum at ~520 nm is consistent with AuNPs of this size, and slight shifts in the plasmon peak are expected due to the change in local refractive index at the surface for the different surface groups.[43] The plasmon bands broaden slightly after functionalization, indicating a small amount of aggregation. The increase in hydrodynamic diameters(d_h) derived from DLS measurements and the ζ-potentials calculated from electrophoretic mobilities for AuNPs in buffer further show the success of AuNPs functionalization (Table S1). TEM images (Figure S2) and the associated histograms (Figure S3) indicate that representative Citrate-AuNPs possessed a core diameter of 14.2 ± 1.6 nm, MTAB-AuNPs 13.9 ± 1.5 nm, PAH-AuNPs 14.5 ± 1.7 nm (n >200).

The data in Table S2 indicate that the hydrodynamic diameters of lipid vesicles range from approximately 70 to 150 nm in diameter on average. We used 100 nm as an average size to estimate the molar concentration of 1 μg mL^{-1} lipid vesicles (see SI for calculation), which is M_{lipid} = 1.27×10^{-6} M. As designed for these experiments, with the addition of 2.4 nM AuNPs, the number ratio of AuNP:lipid vesicle is approximately 150:1, which is also within a range reported previously.[44] Based on their average composition, the ζ-potential of DOPC vesicles and 9:1 DOPC/DOPE vesicles are close to neutral because they are zwitterionic lipids, whereas 9:1 DOPC/DOPS and 9:1 DOPC/DOPG are negatively charged as DOPS and DOPG are both anionic lipids. It is worth mentioning that while extrusion is also a common method for lipid vesicle

production, in our hands it led to more variability in final lipid vesicle concentration than sonication; therefore, we chose sonication over extrusion for making vesicles.

Anionic Citrate-AuNPs interactions with 4 types of lipid vesicles. To validate the hypothesis that electrostatic attraction is one of the main forces driving nanoparticle-lipid vesicle interactions, we incubated anionic Citrate-AuNPs with the anionic lipid vesicles. As shown in Figure 2a, the extinction spectra of Citrate-AuNPs did not exhibit shifts in the plasmon maximum following interaction with any vesicle systems, after redispersion of the pellets after separation from free lipids. A slight broadening at longer wavelengths was observed, possibly due to the aggregation caused by high centrifugation force. No significant changes in hydrodynamic diameters or ζ-potential were observed, and analysis of the LC-MS/MS data by comparing C_{bound}/C_{total} indicated minimal lipid was bound to the Citrate-AuNPs (Figure 2b-d). This data also demonstrates that ~5% or less of the lipids end up in the pellet, if NP-lipid electrostatics are not in favor of lipid-NP binding. Control experiments of lipid vesicles without undergoing the centrifugation process (data not shown) were also compared to the controls being centrifuged, showing that these centrifugation conditions did not sediment lipids (p >0.05, n >30). These data suggested no/little lipid coronas were formed on Citrate-AuNPs, presumably due to the electrostatic repulsion between anionic phospholipids and anionic nanoparticles. (No measurements were made to quantify any citrate desorption, but if lipids simply replaced citrate on the nanoparticles, we would have expected to bind nearly all of the lipids, based on the available surface area of the nanoparticles).

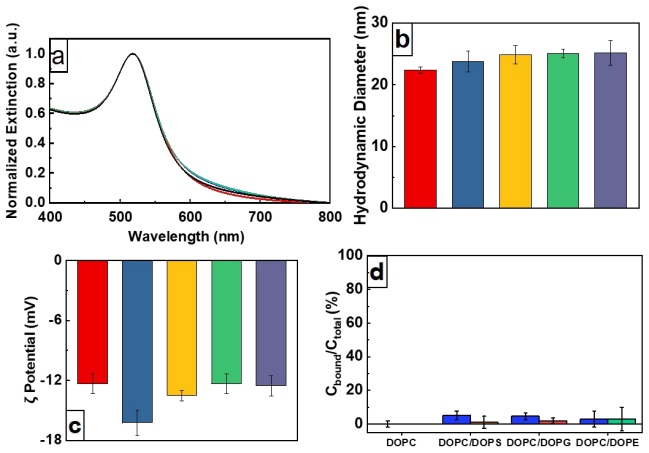

Figure 2. a) UV-vis spectra of Citrate-AuNPs before interaction(red), after interaction with DOPC(blue), 9:1 DOPC/DOPS(green), 9:1 DOPC/DOPG(orange), 9:1 DOPC/DOPE(black); b) DLS and c) ζ-potential of Citrate-AuNPs before interaction (red), after interaction with DOPC (blue), 9:1 DOPC/DOPS (yellow), 9:1 DOPC/DOPG(green), 9:1 DOPC/DOPE(purple); d) LC-MS/MS quantification: C_{bound}/C_{total} (blue: DOPC, red: DOPS, orange: DOPG, green: DOPE). Bar heights represent mean values; error bars correspond to one standard deviation for triplicate runs from the same batches of nanoparticle and lipid vesicle solutions.

Cationic MTAB-AuNPs and PAH-AuNPs interactions with 4 types of lipid vesicles. Incubation experiments of cationic AuNPs were performed to assess the ability of AuNPs to acquire lipid coronas from vesicles. The hydrodynamic diameters and ζ-potentials of AuNPs and vesicles are reported in Table S2("Figure 5 data"). Upon addition of PAH-AuNPs to vesicle solutions, the samples gradually aggregated, leading to sedimentation. In contrast, no visual aggregation was observed for MTAB-AuNPs, despite the similar ζ-potentials of two AuNPs. UV-vis spectra (Figure 3) of the MTAB-AuNPs before and after vesicle incubation and subsequent separation, showed a slight red shift of ~5 nm in the plasmon maximum, suggesting lipid attachment.[45] For PAH-AuNPs, the original peak at ~520 nm was damped, and a new, broadened peak at a longer

wavelength (ranging from 619 to 653 nm) appeared after, indicative of aggregation.[46] These spectroscopic data support the notion that lipid corona formation occurs on MTAB-AuNPs, but for PAH-AuNPs, spectroscopic evidence for lipid corona formation is convoluted with lipid-induced aggregation.

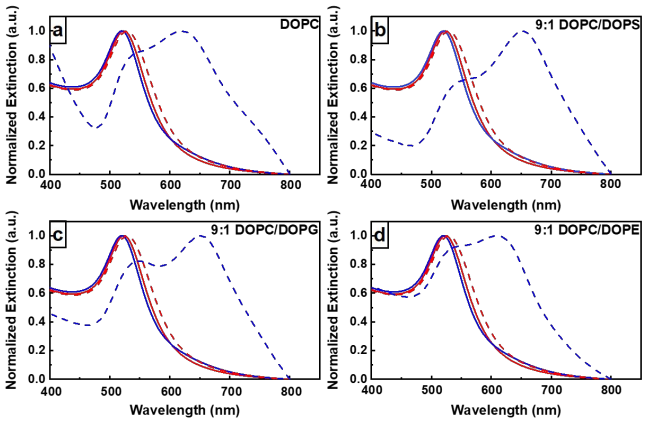

Figure 3. Representative normalized extinction spectra of ~7 nM MTAB-AuNP (red) and PAH-AuNPs (blue) before (solid) and after (dashed) lipid pull-down experiment with a) DOPC, b) 9:1 DOPC/DOPS, c) 9:1 DOPC/DOPG, d) 9:1 DOPC/DOPE.

The hydrodynamic diameters of AuNPs before interaction and lipid-AuNP conjugates after pull-down were measured by DLS. As shown in Figure 4a-d, the hydrodynamic diameters of the MTAB-AuNPs increase by 5-10 nm after addition of vesicles, indicative of the formation of a nanoscale lipid layer(s). A dramatic increase in hydrodynamic diameters of PAH-AuNPs after vesicle incubation, for all lipid systems, indicates aggregation, consistent with both visual observations and UV-vis spectra.

After incubation with DOPC or 9:1 DOPC/DOPE vesicles, the ζ-potentials of both cationic AuNPs did not show drastic changes, which is expected because DOPC and DOPC/DOPE are zwitterionic

(Figure 4e-h). However, the ζ-potentials decreased and switched from positive to negative after interacting with 9:1 DOPC/DOPS or 9:1 DOPC/DOPG, providing compelling evidence for the binding of anionic DOPS or DOPG onto initially cationic AuNPs.

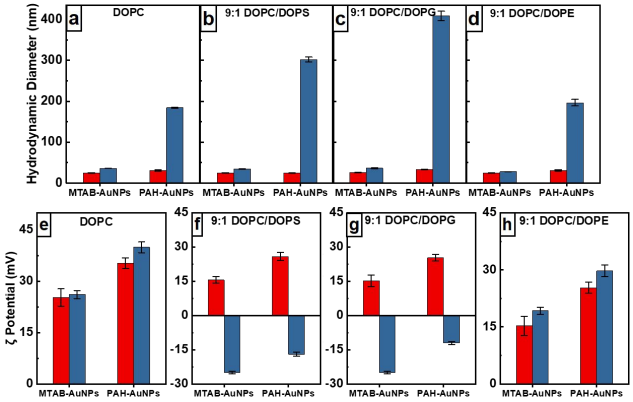

Figure 4. Hydrodynamic diameters and ζ-potential of MTAB- and PAH-AuNPs before (red) and after (blue) lipid pull-down experiments, for lipid vesicles of a/e) DOPC, b/f) 9:1 DOPC/DOPS, c/g) 9:1 DOPC/DOPG, d/h) 9:1 DOPC/DOPE. Bar heights represent mean values; error bars indicate the standard error for 10 runs of DLS analysis or ζ-potential measurements for representative samples.

All the above data qualitatively supports the notion that cationic colloidal nanoparticles can acquire lipids from vesicles. To be more quantitative, lipid concentrations in the supernatants, after nanoparticle pull-down, were measured by LC-MS/MS. Figure S4 shows representative raw data, compared to controls, which underwent the same centrifugation steps as all other samples but contained no nanoparticles. Significant decreases in the amount of lipids in the supernatants were observed for both types of cationic AuNPs in all vesicle systems, indicating the acquisition of lipids from the vesicles by both AuNPs. In Figure 5a, both types of AuNPs bound more than 80% of DOPC under the described conditions, and the amount of DOPC pulled down by the nanoparticles did not differ (p >0.05), indicating a lack of preference of DOPC binding to PAH-

AuNPs or to MTAB-AuNPs. However, when presented with both DOPS and DOPC (Figure 6b), PAH-AuNPs bound more than 95% of both lipids whereas MTAB-AuNPs bound less than 60% of lipids, with a strong preference for anionic DOPS relative to zwitterionic DOPC. Similar, but not identical, results were obtained for 9:1 DOPC/DOPG anionic vesicles (Figure 6c): PAH-AuNPs bound more lipids than MTAB-AuNPs. For zwitterionic 9:1 DOPC/DOPE vesicles, the two types of nanoparticles pulled down 85-95% of both lipids. Table S2 lists the characteristics for each batch of vesicles and nanoparticles for each data set in Figure 5.

While these data themselves to not provide direct binding affinities for lipid-nanoparticle interactions, in initial experiments (data not shown) we found that 3X lower vesicle concentrations than the ones described above led to complete lipid pulldown by PAH-AuNPs. Related experiments from our group suggest that cationic gold nanoparticles irreversibly adsorb to supported lipid bilayers with ~1 x 10^{11} particles/cm^2, albeit under different conditions and for DOPC with a different co-lipid. [28] Taken together, these data provide qualitative context for the relative strength of lipid-NP interactions. Another question that might arise is: do the lipids replace MTAB and PAH on the particle surface, or do they merely associate with the surface-bound ligands? In the absence of quantitative data in which free MTAB or PAH is measured in supernatants, we suggest that lipid replacement is unlikely due to the strong Au-S bonds and hydrophobic tail interactions in the case of MTAB, and the multivalent electrostatic points of contact in the case of PAH. The surface chemistry and DLS/zeta potential data, taken together, suggest that the assumption of lipid acquisition by nanoparticles with intact surface ligands is a reasonable one.

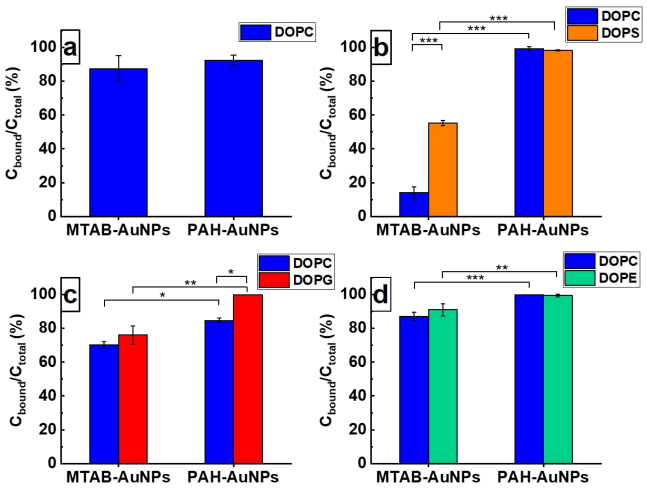

Figure 5. C_{bound}/C_{total} percentage, after pull-down separation of AuNP pellets, based on LC-MS/MS quantification. The lipids are a) DOPC, b) 9:1 DOPC/DOPS, c) 9:1 DOPC/DOPG, d) 9:1 DOPC/DOPE. Bar heights represent mean values; error bars correspond to one standard deviation for triplicate runs from the same batches of nanoparticle and lipid vesicle solutions. The nanoparticle batches were independently synthesized for a, b, c, d, as were the lipid vesicle solutions. Asterisks correspond to the following *p* values using ANOVA followed by post hoc multiple comparisons test: * $p < 0.05$; ** $p < 0.01$, *** $p < 0.001$.

Batch-to-batch variation in zeta potential and hydrodynamic size does occur for both nanoparticles and lipid vesicles (Table S2, Figure S5). An example of analogous results for Figure 5, but with an unusual batch of MTAB-AuNPs (+ 46 mV zeta potential compared to the usual +15 mV; Figure S6b) shows that while the absolute magnitude of lipid pull-down is altered (more positive zeta potential does lead to more lipid binding), the general trends of Figure 5 are robust, and more lipids are pulled down by PAH-AuNPs compared to MTAB-AuNP, while very little are pulled down by

the anionic citrate-capped nanoparticles. The natural assumption is that electrostatic interactions dominate relations between vesicles and nanoparticles.[47] This is perhaps obvious, but the chemical nature of MTAB and PAH are quite different. For example, the quaternary ammonium headgroup of MTAB is a poor hydrogen bond donor or acceptor compared to PAH, whereas the hydrophobicity of MTAB is higher than PAH due to its C16 chain, which one could have postulated would have resulted in favorable hydrophobic interactions with the hydrophobic tails of lipids.[40] Furthermore, MTAB is a classic example of a self-assembled thiol on a gold surface via Au-S bonds, and is expected to display a rather packed, uniform cationic surface to the solvent. PAH, on the other hand, is a polymer that is electrostatically associated with the nanoparticle core, and, according to NMR experiments of it bound to other nanoparticles, it has segments farther away from the surface and in highly mobile environments (loops and tails).[57] The mobility of polymer segments or ligands on nanoparticles may potentially affect how they interact with lipid vesicles. [13, 57] It also has been reported previously that polymers bearing primary amines exceed their quaternary ammonium counterparts in membrane binding and disruption.[48] In spite of the many contributors to the thermodynamics of lipid-nanoparticle interactions that make quantitative predictions difficult (charge density, water and ion local concentrations, hydrophobic and electrostatic interactions, hydrogen bonding), we conclude that the primary amine, "loopy" surface of PAH is more likely to pull lipids out from vesicles than the quaternary ammonium "uniform" surface of MTAB .[49]

A large amount of evidence shows that cationic nanoparticles have more adverse outcomes than their anionic counterpart at the cellular level.[12,37,50] The evidence we present, that lipids are quantitatively extracted from vesicles by cationic nanoparticles, may provide a mechanism at the

cellular level: lipid extraction from membranes by nanoparticles would disrupt the cell membranes and induce membrane damage which can eventually lead to cell death.[51,52] While MTAB-AuNPs have shown an excellent ability to be taken up by cells, the toxicity of MTAB itself to biological systems has not been reported yet,[53,54] but PAH seems to be rather cytotoxic.[47,55,56]

Effects of purification method of AuNPs and other ratios of AuNPs:lipid vesicles. The purification method of the nanomaterials used in this study above was twice-centrifugation. This rigorous purification scheme was chosen because it was found that an extra round of centrifugation can further reduce the amount of unbound PAH polymer in the nanoparticle solution by an order of magnitude, which eliminates most of the free PAH, resulting in a relatively clean system.[56] However, we noticed that PAH-AuNPs are less stable than MTAB-AuNPs, and they eventually aggregated in buffer after ~2 days. As a 1× centrifugation of PAH-AuNPs leads to more stable colloidal suspensions (but also leaves measurable quantities of free PAH in the supernatant), we also quantified the lipids pulled down by both MTAB- and PAH-AuNPs purified with 1× centrifugation. In these experiments, 500 µL 4.8 nM AuNPs were added, respectively, in 500 µL 2, 20, or 200 µg mL^{-1} (at number ratio of 150:1, 15:1, 1.5:1) of two vesicles system (9:1 DOPC/DOPS, 9:1 DOPC/DOPG), and underwent the same process of pull-down experiment as above described.

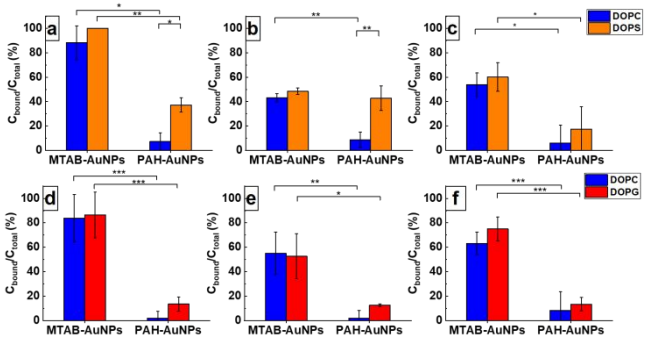

Figure 6. C_{bound}/C_{total} percentage, after pull-down separation of AuNP pellets, based on LC-MS/MS quantification, for 9:1 DOPC/DOPS (a-c) and 9:1 DOPC/DOPG (d-f), for 4.8 nM MTAB- and PAH- AuNPs interacting with a/d) 2 μg mL^{-1}, b/e) 20 μg mL^{-1}, c/f) 200 μg mL^{-1} lipid vesicles, compared to controls. Bar heights represent mean values; error bars correspond to one standard deviation, n = 3, for three batches of nanoparticles and one batch of lipid vesicles. Asterisks correspond to the following p values using ANOVA followed by post hoc multiple comparisons test: * p <0.05; ** p <0.01, *** p <0.001.

With a competitor in the supernatant for lipids – free PAH - the comparison between MTAB-AuNPs and PAH-AuNPs is tilted far in apparent favor of MTAB, meaning PAH-AuNPs acquired much less lipids. The likely reason for the significant change in lipid association with the PAH-AuNPs is that free PAH (7.53 mg L^{-1} per mg L^{-1} in supernatants of 1x centrifuged AuNPs, instead of 0.49 mg L^{-1} in supernatants of 2x centrifuges AuNPs)[56] sequesters lipids and competes with PAH bound to nanoparticles. In this circumstance, lipids appear to prefer free PAH compared to nanoparticle-bound PAH. Details of the conformation of free PAH and bound PAH are doubtless involved in this discrimination, as well as considerations of possible differences in the relative binding energies of lipid/free PAH compared to lipid/bound PAH;[57,58] we note that previous NMR experiments of 4 nm PAH-AuNPs suggested that the PAH polymer is "loosened" upon lipid vesicle interaction.[28] The other interesting point about the data in Figure 6 is that even though lipid concentrations are increasing 100×, C_{bound}/C_{total} is only modestly affected, meaning absolutely more lipids are bound and are likely forming multilayers on cationic NP surfaces, similar to what we have observed before for both PAH and hydrophobic particle surfaces.[18]

CONCLUSION

In summary, we developed a centrifugation-based pull-down assay in which one anionic AuNP and two cationic AuNPs were incubated with four lipid vesicles systems. Collective data demonstrate both qualitatively and quantitively that phospholipids in vesicles are extracted and bound to cationic AuNPs, indicating a lipid corona formation on both types of cationic AuNPs. Little lipid corona was formed on Citrate-AuNPs, supporting the electrostatic nature of the interactions. Different degrees of binding to both cationic AuNPs were observed in the binary vesicles systems, and different compositions of lipids may lead to different lipid coronas, independent of abundance of lipids. In the binary vesicle systems, the quantitative data show that PAH-AuNPs has higher tendency to extract lipids from the vesicles. We also note that insufficient purification of nanoparticle solutions can lead to free ligand, which competes for lipid binding and can give erroneous conclusions about NP-lipid affinities.

With the promising, though challenging, development of lipidomics by LC-MS/MS, we envision the work presented herein setting the stage for generation of a "lipid corona fingerprinting" database by quantitatively correlating lipid corona information to cellular uptake, membrane disruption, trafficking and cytotoxicity, to improve quantitative predictions of nano-bio interactions.[32,59]

ACKNOWLEDGEMENTS

We thank the NSF Center for Sustainable Nanotechnology (Grant CHE-1503408) and its members for support, especially Professors Joel Pedersen and Christy Haynes. We thank Dr. Lucas Li,

Metabolomics Laboratory of the Roy J. Carver Biotechnology Center at UIUC, for the raw data of lipid quantification.

Supporting Information Available: Representative extinction spectra, TEM images and diameter histograms, λ_{max}, d_h, and ζ-potentials of citrate-AuNPs, MTAB-AuNPs and PAH-AuNPs; Raw quantification of lipids in the supernatants by LC-MS/MS; d_h and ζ-potentials of two batches of lipid vesicles, MTAB-AuNPs and PAH-AuNPs used in different systems; batch-to-batch reproducibility data; LC-MS/MS method; Calculation of the number ratio of AuNPs:lipid vesicles; ζ-potentials of 16 batches of MTAB-AuNPs; MTAB synthesis and characterization.

REFERENCES

(1) Murphy, C. J.; Sau, T. K.; Gole, A. M.; Orendorff, C. J.; Gao, J.; Gou, L.; Hunyadi, S. E.; Li, T. Anisotropic Metal Nanoparticles: Synthesis, Assembly, and Optical Applications. *J. Phys. Chem. B* **2005**, *109*, 13857–13870.

(2) Saha, K.; Agasti, S. S.; Kim, C.; Li, X.; Rotello, V. M. Gold Nanoparticles in Chemical and Biological Sensing. *Chem. Rev.* **2012**, *112*, 2739–2779.

(3) Murphy, C. J.; Gole, A. M.; Stone, J. W.; Sisco, P. N.; Alkilany, A. M.; Goldsmith, E. C.; Baxter, S. C. Gold Nanoparticles in Biology: Beyond Toxicity to Cellular Imaging. *Acc. Chem. Res.* **2008**, *41*, 1721–1730.

(4) Ghosh, P.; Han, G.; De, M.; Kim, C. K.; Rotello, V. M. Gold Nanoparticles in Delivery Applications. *Adv. Drug Deliv. Rev.* **2008**, *60*, 1307–1315.

(5) Jain, S.; Hirst, D. G.; O'Sullivan, J. M. Gold Nanoparticles as Novel Agents for Cancer Therapy. *Br. J. Radiol.* **2012**, *85*, 101–113.

(6) Dreaden, E. C.; Alkilany, A. M.; Huang, X.; Murphy, C. J.; El-Sayed, M. A. The Golden Age: Gold Nanoparticles for Biomedicine. *Chem. Soc. Rev.* **2012**, *41*, 2740–2779.

(7) Abadeer, N. S.; Murphy, C. J. Recent Progress in Cancer Thermal Therapy Using Gold Nanoparticles. *J. Phys. Chem. C* **2016**, *120*, 4691–4716.

(8) Verma, A.; Stellacci, F. Effect of Surface Properties on Nanoparticle-Cell Interactions. *Small* **2010**, *6*, 12–21.

(9) Albanese, A.; Tang, P. S.; Chan, W. C. W. The Effect of Nanoparticle Size, Shape, and Surface Chemistry on Biological Systems. *Annu. Rev. Biomed. Eng.* **2012**, *14*, 1–16.

(10) Fadeel, B.; Garcia-Bennett, A. E. Better Safe than Sorry: Understanding the Toxicological Properties of Inorganic Nanoparticles Manufactured for Biomedical Applications. *Adv. Drug Deliv. Rev.* **2010**, *62*, 362–374.

(11) Guzmán, K. A. D.; Taylor, M. R.; Banfield, J. F. Environmental Risks of Nanotechnology: National Nanotechnology Initiative Funding, 2000-2004. *Environ. Sci. Technol.* **2006**, *40*, 1401–1407.

(12) Murphy, C. J.; Vartanian, A. M.; Geiger, F. M.; Hamers, R. J.; Pedersen, J.; Cui, Q.; Haynes, C. L.; Carlson, E. E.; Hernandez, R.; Klaper, R. D.; Orr, G.; Rosenzweig, Z. Biological Responses to Engineered Nanomaterials: Needs for the next Decade. *ACS Cent. Sci.* **2015**, *1*, 117–123.

(13) Nel, A. E.; Mädler, L.; Velegol, D.; Xia, T.; Hoek, E. M. V.; Somasundaran, P.; Klaessig, F.; Castranova, V.; Thompson, M. Understanding Biophysicochemical Interactions at the Nano-Bio Interface. *Nat. Mater.* **2009**, *8*, 543–557.

(14) Gagner, J. E.; Shrivastava, S.; Qian, X.; Dordick, J. S.; Siegel, R. W. Engineering Nanomaterials for Biomedical Applications Requires Understanding the Nano-Bio Interface: A Perspective. *J. Phys. Chem. Lett.* **2012**, *3*, 3149–3158.

(15) Docter, D.; Westmeier, D.; Markiewicz, M.; Stolte, S.; Knauer, S. K.; Stauber, R. H. The Nanoparticle Biomolecule Corona: Lessons Learned - Challenge Accepted? *Chem. Soc. Rev.* **2015**, *44*, 6094–6121.

(16) Calzolai, L.; Franchini, F.; Gilliland, D.; Rossi, F. Protein-Nanoparticle Interaction: Identification of the Ubiquitin-Gold Nanoparticle Interaction Site. *Nano Lett.* **2010**, *10*, 3101–3105.

(17) Melby, E. S.; Lohse, S. E.; Park, J. E.; Vartanian, A. M.; Putans, R. A.; Abbott, H. B.; Hamers, R. J.; Murphy, C. J.; Pedersen, J. A. Cascading Effects of Nanoparticle Coatings: Surface Functionalization Dictates the Assemblage of Complexed Proteins and Subsequent Interaction with Model Cell Membranes. *ACS Nano* **2017**, *11*, 5489–5499.

(18) Yang, J. A.; Murphy, C. J. Evidence for Patchy Lipid Layers on Gold Nanoparticle Surfaces. *Langmuir* **2012**, *28*, 5404–5416.

(19) Raesch, S. S.; Tenzer, S.; Storck, W.; Rurainski, A.; Selzer, D.; Ruge, C. A.; Perez-Gil, J.; Schaefer, U. F.; Lehr, C. M. Proteomic and Lipidomic Analysis of Nanoparticle Corona upon Contact with Lung Surfactant Reveals Differences in Protein, but Not Lipid Composition. *ACS Nano* **2015**, *9*, 11872–11885.

(20) Hu, M.; Stanzione, F.; Sum, A. K.; Faller, R.; Deserno, M. Design Principles for Nanoparticles Enveloped by a Polymer-Tethered Lipid Membrane. *ACS Nano* **2015**, *9*, 9942–9954.

(21) Van Lehn, R. C.; Alexander-Katz, A. Fusion of Ligand-Coated Nanoparticles with Lipid

Bilayers: Effect of Ligand Flexibility. *J. Phys. Chem. A* **2014**, *118*, 5848–5856.

(22) Van Lehn, R. C.; Alexander-Katz, A. Structure of Mixed-Monolayer-Protected Nanoparticles in Aqueous Salt Solution from Atomistic Molecular Dynamics Simulations. *J. Phys. Chem. C* **2013**, *117*, 20104–20115.

(23) Edidin, M. Lipids on the Frontier: A Century of Cell-Membrane Bilayers. *Nat. Rev. Mol. Cell Biol.* **2003**, *4*, 414–418.

(24) Hou, W.-C.; Moghadam, B. Y.; Corredor, C.; Westerhoff, P.; Posner, J. D. Distribution of Functionalized Gold Nanoparticles between Water and Lipid Bilayers as Model Cell Membranes. *Environ. Sci. Technol.* **2012**, *46*, 1869–1876.

(25) Roiter, Y.; Ornatska, M.; Rammohan, A. R.; Balakrishnan, J.; Heine, D. R.; Minko, S. Interaction of Nanoparticles with Lipid Membrane. *Nano Lett.* **2008**, *8*, 941–944.

(26) Van Lehn, R. C.; Atukorale, P. U.; Carney, R. P.; Yang, Y. S.; Stellacci, F.; Irvine, D. J.; Alexander-Katz, A. Effect of Particle Diameter and Surface Composition on the Spontaneous Fusion of Monolayer-Protected Gold Nanoparticles with Lipid Bilayers. *Nano Lett.* **2013**, *13*, 4060–4067.

(27) Chen, K. L.; Bothun, G. D. Nanoparticles Meet Cell Membranes: Probing Nonspecific Interactions Using Model Membranes. *Environ. Sci. Technol.* **2014**, *48*, 873–880.

(28) Troiano, J. M.; Olenick, L. L.; Kuech, T. R.; Melby, E. S.; Hu, D.; Lohse, S. E.; Mensch, A. C.; Dogangun, M.; Vartanian, A. M.; Torelli, M. D.; Ehimiaghe, E.; Walter, S. R.; Fu, L.; Anderton, C. R.; Zhu, Z.; Wang, H.; Orr, G.; Murphy, C. J.; Hamers, R. J.; Pedersen, J. A.; Geiger, F. M. Direct Probes of 4 nm Diameter Gold Nanoparticles Interacting with Supported Lipid Bilayers. *J. Phys. Chem. C* **2015**, *119*, 534–546.

(29) Olenick, L. L.; Troiano, J. M.; Vartanian, A.; Melby, E. S.; Mensch, A. C.; Zhang, L.; Hong,

J.; Qiu, T.; Bozich, J.; Lohse, S.; Zhang, X.; Kuech, T. R.; Millevolte, A.; Gunsolus, I.; McGeachy, A. C.; Dogangun, M.; Li, T.; Hu, D.; Walter, S. R.; Mohaimani, A.; Schmoldt, A.; Torelli, M. D.; Hurley, K. R.; Dalluge, J.; Chong, G.; Feng, Z. V.; Haynes, C. L.; Hamers, R. J.; Pedersen, J. A.; Cui, Q.; Hernandez, R.; Klaper, R.; Orr, G.; Murphy, C. J.; Geiger, F. Lipid Corona Formation from Nanoparticle Interactions with Bilayers and Membrane-Specific Biological Outcomes. **2017**, https://doi.org/10.26434/chemrxiv.5512996.v1.

(30) Bekdemir, A.; Stellacci, F. A Centrifugation-Based Physicochemical Characterization Method for the Interaction between Proteins and Nanoparticles. *Nat. Commun.* **2016**, *7*, 13121.

(31) Xi, A.; Bothun, G. D. Centrifugation-Based Assay for Examining Nanoparticle-Lipid Membrane Binding and Disruption. *Analyst* **2014**, *139*, 973–981.

(32) Walkey, C. D.; Olsen, J. B.; Song, F.; Liu, R.; Guo, H.; Olsen, D. W. H.; Cohen, Y.; Emili, A.; Chan, W. C. W. Protein Corona Fingerprinting Predicts the Cellular Interaction of Gold and Silver Nanoparticles. *ACS Nano* **2014**, *8*, 2439–2455.

(33) Vigderman, L.; Manna, P.; Zubarev, E. R. Quantitative Replacement of Cetyl Trimethylammonium Bromide by Cationic Thiol Ligands on the Surface of Gold Nanorods and Their Extremely Large Uptake by Cancer Cells. *Angew. Chemie - Int. Ed.* **2012**, *51*, 636–641.

(34) Turkevich, J.; Stevenson, P. C.; Hillier, J. A Study of the Nucleation and Growth Processes in the Synthesis of Colloidal Gold. *Discuss. Faraday Soc.* **1951**, *11*, 55–75.

(35) Haiss, W.; Thanh, N. T. K.; Aveyard, J.; Fernig, D. G. Determination of Size and Concentration of Gold Nanoparticles from UV-Vis Spectra. *Anal. Chem.* **2007**, *79*, 4215–4221.

(36) Buchman, J. T.; Rahnamoun, A.; Landy, K. M.; Zhang, X.; Vartanian, A. M.; Jacob, L. M.; Murphy, C. J.; Hernandez, R.; Haynes, C. L. Using an Environmentally-Relevant Panel of Gram-Negative Bacteria to Assess the Toxicity of Polyallylamine Hydrochloride-Wrapped Gold Nanoparticles. *Environ. Sci. Nano* **2018**, *5*, 279–288.

(37) Bozich, J. S.; Lohse, S. E.; Torelli, M. D.; Murphy, C. J.; Hamers, R. J.; Klaper, R. D. Surface Chemistry, Charge and Ligand Type Impact the Toxicity of Gold Nanoparticles to Daphnia Magna. *Environ. Sci. Nano* **2014**, *1*, 260–270.

(38) Troiano, J. M.; McGeachy, A. C.; Olenick, L. L.; Fang, D.; Liang, D.; Hong, J.; Kuech, T. R.; Caudill, E. R.; Pedersen, J. A.; Cui, Q.; Geiger, F. M. Quantifying the Electrostatics of Polycation–Lipid Bilayer Interactions. *J. Am. Chem. Soc.* **2017**, *139*, 5808–5816.

(39) Yang, J. A.; Lin, W.; Woods, W. S.; George, J. M.; Murphy, C. J. α-Synuclein's Adsorption, Conformation, and Orientation on Cationic Gold Nanoparticle Surfaces Seeds Global Conformation Change. *J. Phys. Chem. B* **2014**, *118*, 3559–3571.

(40) Lin, W.; Insley, T.; Tuttle, M. D.; Zhu, L.; Berthold, D. A.; Král, P.; Rienstra, C. M.; Murphy, C. J. Control of Protein Orientation on Gold Nanoparticles. *J. Phys. Chem. C* **2015**, *119*, 21035–21043.

(41) Geiger, O.; López-Lara, I. M.; Sohlenkamp, C. Phosphatidylcholine Biosynthesis and Function in Bacteria. *Biochim. Biophys. Acta - Mol. Cell Biol. Lipids* **2013**, *1831*, 503–513.

(42) Martínez-Morales, F.; Schobert, M.; López-Lara, I. M.; Geiger, O. Pathways for Phosphatidylcholine Biosynthesis in Bacteria. *Microbiology* **2003**, *149*, 3461–3471.

(43) Ghosh, S. K.; Pal, T. Interparticle Coupling Effect on the Surface Plasmon Resonance of Gold Nanoparticles: From Theory to Applications. *Chem. Rev.* **2007**, *107*, 4797–4862.

(44) Wang, B.; Zhang, L.; Bae, S. C.; Granick, S. Nanoparticle-Induced Surface Reconstruction

of Phospholipid Membranes. *Proc. Natl. Acad. Sci.* **2008**, *105*, 18171–18175.

(45) Van Lehn, R. C.; Ricci, M.; Silva, P. H. J.; Andreozzi, P.; Reguera, J.; Voïtchovsky, K.; Stellacci, F.; Alexander-Katz, A. Lipid Tail Protrusions Mediate the Insertion of Nanoparticles into Model Cell Membranes. *Nat. Commun.* **2014**, *5*, 4482.

(46) Su, K. H.; Wei, Q. H.; Zhang, X.; Mock, J. J.; Smith, D. R.; Schultz, S. Interparticle Coupling Effects on Plasmon Resonances of Nanogold Particles. *Nano Lett.* **2003**, *3*, 1087–1090.

(47) Torrano, A. A.; Pereira, Â. S.; Oliveira, O. N.; Barros-Timmons, A. Probing the Interaction of Oppositely Charged Gold Nanoparticles with DPPG and DPPC Langmuir Monolayers as Cell Membrane Models. *Colloids Surfaces B Biointerfaces* **2013**, *108*, 120–126.

(48) Palermo, E. F.; Lee, D. K.; Ramamoorthy, A.; Kuroda, K. Role of Cationic Group Structure in Membrane Binding and Disruption by Amphiphilic Copolymers. *J. Phys. Chem. B* **2011**, *115*, 366–375.

(49) De, M.; You, C. C.; Srivastava, S.; Rotello, V. M. Biomimetic Interactions of Proteins with Functionalized Nanoparticles: A Thermodynamic Study. *J. Am. Chem. Soc.* **2007**, *129*, 10747–10753.

(50) Fröhlich, E. The Role of Surface Charge in Cellular Uptake and Cytotoxicity of Medical Nanoparticles. *Int. J. Nanomedicine* **2012**, *7*, 5577–5591.

(51) Van Lehn, R. C.; Alexander-Katz, A. Penetration of Lipid Bilayers by Nanoparticles with Environmentally-Responsive Surfaces: Simulations and Theory. *Soft Matter* **2011**, *7*, 11392.

(52) Cheng, X.; Zhang, W.; Ji, Y.; Meng, J.; Guo, H.; Liu, J.; Wu, X.; Xu, H. Revealing Silver Cytotoxicity Using Au Nanorods/Ag Shell Nanostructures: Disrupting Cell Membrane and Causing Apoptosis through Oxidative Damage. *RSC Adv.* **2013**, *3*, 2296–2305.

(53) Wang, C.; Sun, A.; Qiao, Y.; Zhang, P.; Ma, L.; Su, M. Cationic Surface Modification of Gold Nanoparticles for Enhanced Cellular Uptake and X-Ray Radiation Therapy. *J. Mater. Chem. B* **2015**, *3*, 7372–7376.

(54) Zarska, M.; Novotny, F.; Havel, F.; Sramek, M.; Babelova, A.; Benada, O.; Novotny, M.; Saran, H.; Kuca, K.; Musilek, K.; Hvezdova, Z.; Dzijak, R.; Vancurova, M.; Krejcikova, K.; Gabajova, B.; Hanzlikova, H.; Kyjacova, L.; Bartek, J.; Proska, J.; Hodny, Z. Two-Step Mechanism of Cellular Uptake of Cationic Gold Nanoparticles Modified by (16-Mercaptohexadecyl)Trimethylammonium Bromide. *Bioconjug. Chem.* **2016**, *27*, 2558–2574.

(55) Feng, Z. V.; Gunsolus, I. L.; Qiu, T. A.; Hurley, K. R.; Nyberg, L. H.; Frew, H.; Johnson, K. P.; Vartanian, A. M.; Jacob, L. M.; Lohse, S. E.; Torelli, M. D.; Hamers, R. J.; Murphy, C. J.; Haynes, C. L. Impacts of Gold Nanoparticle Charge and Ligand Type on Surface Binding and Toxicity to Gram-Negative and Gram-Positive Bacteria. *Chem. Sci.* **2015**, *6*, 5186–5196.

(56) Qiu, T. A.; Torelli, M. D.; Vartanian, A. M.; Rackstraw, N. B.; Buchman, J. T.; Jacob, L. M.; Murphy, C. J.; Hamers, R. J.; Haynes, C. L. Quantification of Free Polyelectrolytes Present in Colloidal Suspension, Revealing a Source of Toxic Responses for Polyelectrolyte-Wrapped Gold Nanoparticles. *Anal. Chem.* **2017**, *89*, 1823–1830.

(57) Zhang, Y.; Fry, C. G.; Pedersen, J. A.; Hamers, R. J. Dynamics and Morphology of Nanoparticle-Linked Polymers Elucidated by Nuclear Magnetic Resonance. *Anal. Chem.* **2017**, *89*, 12399–12407.

(58) Chong, G.; Hernandez, R. Adsorption Dynamics and Structure of Polycations on Citrate-Coated Gold Nanoparticles. *J. Phys. Chem. C* **2018**, *122*, 19962–19969.

(59) Köfeler, H. C.; Fauland, A.; Rechberger, G. N.; Trötzmüller, M. Mass Spectrometry Based Lipidomics: An Overview of Technological Platforms. *Metabolites* **2012**, *2*, 19–38.

For TOC only